CHAPTER III

SINGULAR ELEMENT SHAPE FUNCTION

One of contributions of the research, that is applying the singular element shape function onto the combined finite element and moment methods in the analysis of the edge slot, is discussed in this chapter. The basic formulation is confined and followed by its implementation in the analysis. The cavity integral for the singular element which can not be solved analytically is evaluated by using the Gauss quadrature integral approximation for a triangular area. The three-dimensional singular element shape function is also modified into two dimensional form to be applied on the internal surface integrals.

3.1 Finite element on singular point

The FEM exhibits a slow rate of convergence when it is used in the analysis of the waveguide involving sharp edge where the electromagnetic field is singular. There are two classes of solutions to encounter this problem, namely the direct method and the singular element formulation.

The first method is utilized by applying a straightforward finite element method using the standard element and reducing the size of the element near the region containing the singularity. This method is simpler than the second one, since it still uses a standard code. However, it needs a very large number of degrees of freedom to achieve results with a reasonable accuracy.

The second method is utilized by using similar meshing dimension and applying the special formulation, namely singular element shape function, in which the element contains at least one singular point. This formulation describes more accurately than the standard element in the node related with the singular point. Therefore, the accuracy will be increased without enlarging the degree of freedom.

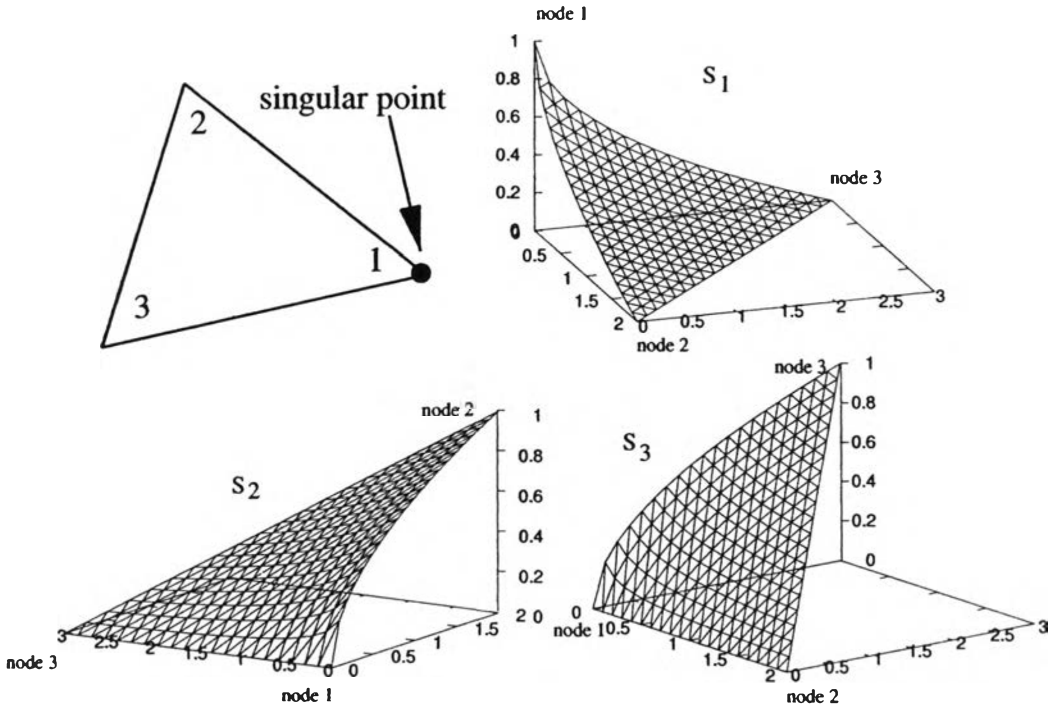

Figure 3.1: The singular element shape function.

There are several different formulations suggested in this concept. However, since the singular element has neighbor standard element, the interpolation function must be compatible with those adjoining standard elements.

3.2 Formulation of singular element shape function

The research employs the singular element shape function that proposed by J.E. Akin [16]. A singular element, whose node 1 lies on the singular corner, has the specific shape function as follows.

$$\begin{aligned} S_1 &= 1-(1-L_1)^{1-\rho} \\ S_2 &= \frac{L_2}{(1-L_1)^{\rho}} \\ S_3 &= \frac{L_3}{(1-L_1)^{\rho}} \end{aligned} \tag{3.1}$$

in which L_i is the area coordinate of node i as expressed in equation (2.27). The factor ρ denotes the order of the desired derivative singularity. It has value in the range from zero to unity, as depicted in Fig. 3.1. When $\rho = 0$ the function becomes

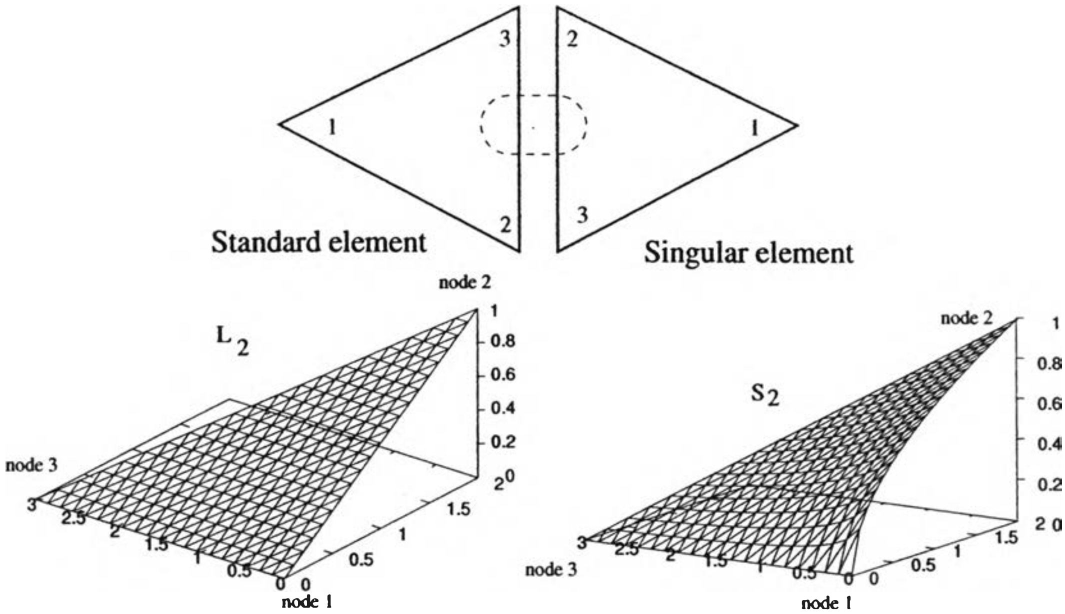

Figure 3.2: The adjoining of singular element and standard element shape functions

similar with the standard shape function.

The function of S_i is unity at the origin node i and vanishes at the other nodes. It is noted that the shape function should satisfy the condition that

$$S_1 + S_2 + S_3 = 1. \tag{3.2}$$

In the implementation of the singular element shape function on the analysis, it replaces the shape function just for the elements near the singular corner and keep the others as the standard element. Thus, the shape functions must have a good adjoining each other. Fig. 3.2 shows that both of the functions on the appropriate neighboring side of the element are linear. It can be used to prove that the Akin's formulations satisfies the condition of a good adjoint with the standard element.

Many studies proved that the Akin's posses a good capability to handle the singularity problem and improves the accuracy and convergency of the analysis. As an example, it could work well on the mode analysis of the ridge and L-shape waveguides , as reported in [24]. Therefore, it motivated to be applied on the analysis of edge slot, as done in this research.

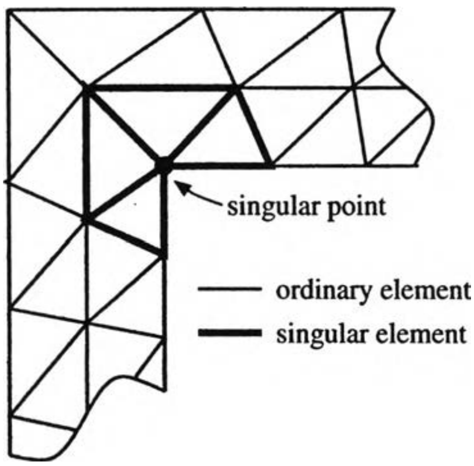

Figure 3.3: The configuration of singular element on the cavity's corner

3.3 Elaborating the singular element on the analysis of edge slot

The structure of the edge slot is cut on the narrow wall of a rectangular waveguide and extended onto the broad wall. Two corners due to the waveguide corners cause a singularity problem when it is analyzed by FEM. Therefore, the singular element shape function is proposed to be elaborated to overcome this problem.

The singular element is utilized in each corner as depicted in Fig. 3.3. The node on the corner is defined as a singular node in each singular element. Then, the shape function on those elements is replaced by the singular element shape function and keep on the standard element for the other elements.

The use of the new shape function needs a modification in the derivation of the integral for the cavity for all singular elements and the integrals of internal surface for the elements that have two nodes on this surface. The derivation is discussed in the next two subsections.

3.3.1 Singular element on the cavity integral

Initially, the unknown in the integral of the cavity region in (2.25) is expanded in term of singular element shape function.

$$\phi(\bar{r}) = \sum_{i=1}^{3} \phi_i^{(e)} S_i(\bar{r}) \tag{3.3}$$

where S_i's are the singular element nodal function expressed in (3.1) and we get two integrals that must be solved.

$$G_{ij}^{(e_{singular})} = w \iint_{A^e} S_i S_j \, dA^e + \frac{w}{k^2} \iint_{A^e} \nabla S_i \cdot \nabla S_j \, dA^e \tag{3.4}$$

Hence, the ρ-quadratic form of the shape function makes the integrals difficult to solve analytically. Therefore, the integrals are proceed by employing the Gaussian or Gauss-Legendre quadrature numerical integration. The detail explanation of this numerical approximation is enclosed in the Appendix.

The procedure of the calculation is begun by transforming the coordinate of the real element into a reference element coordinate, notated as ξ, η. The standard shape function L_i whose value is unity in node-i and zero on other nodes uses as the form function in this geometrical transformation and we get the expression of the singular element shape function in term of reference element coordinate (ξ, η).

$$\begin{aligned} S_1 &= 1 - (\xi + \eta)^{(1-\rho)} \\ S_2 &= \frac{\xi}{(\xi + \eta)^{\rho}} \\ S_3 &= \frac{\eta}{(\xi + \eta)^{\rho}} \end{aligned} \tag{3.5}$$

The first integral of (3.4) can be expressed in the reference coordinate and evaluated by using the Gauss quadrature.

$$\begin{aligned} w \iint_{A_e} S_i(\bar{r}) S_j(\bar{r}) \, dA_e &= w \int_0^1 \int_0^{1-\xi} S_i(\xi, \eta) S_j(\xi, \eta) \, d\eta d\xi \\ &= w|J| \cdot \sum_{i=1}^{n} w_i S_i(\xi, \eta) S_j(\xi, \eta) \end{aligned} \tag{3.6}$$

where (ξ_i, η_i), and w_i are the sample points of the gauss quadrature and their weighting value respectively that can be found in the table in the Appendix, and $|J|$ is the determinant of the Jacobian transformation that is defined as

$$J = \begin{bmatrix} \frac{\partial x}{\partial \xi} & \frac{\partial y}{\partial \xi} \\ \frac{\partial x}{\partial \eta} & \frac{\partial y}{\partial \eta} \end{bmatrix} = \begin{bmatrix} x_2 - x_1 & y_2 - y_1 \\ x_3 - x_1 & y_3 - y_1 \end{bmatrix} \tag{3.7}$$

$$|J| = (x_2 - x_1)(y_3 - y_1) - (x_3 - x_1)(y_2 - y_1) = 2A_e \tag{3.8}$$

Proceeding further, the chain rule is applied to derive the gradient of the scalar shape function in the second integral of (3.4).

$$\nabla\phi = \frac{\partial\phi}{\partial x}\hat{a}_x + \frac{\partial\phi}{\partial y}\hat{a}_y \tag{3.9}$$

$$\nabla\phi = \left(\frac{\partial\phi}{\partial\xi}\cdot\frac{\partial\xi}{\partial x} + \frac{\partial\phi}{\partial\eta}\cdot\frac{\partial\eta}{\partial x}\right)\hat{a}_x + \left(\frac{\partial\phi}{\partial\xi}\cdot\frac{\partial\xi}{\partial y} + \frac{\partial\phi}{\partial\eta}\cdot\frac{\partial\eta}{\partial y}\right)\hat{a}_y \tag{3.10}$$

The first derivatives of S_i over the ξ and η are defined as follows.

$$\frac{\partial S_1}{\partial\xi} = \frac{\rho-1}{(\xi+\eta)^\rho} \tag{3.11}$$

$$\frac{\partial S_1}{\partial\eta} = \frac{\rho-1}{(\xi+\eta)^\rho} \tag{3.12}$$

$$\frac{\partial S_2}{\partial\xi} = \frac{\xi+\eta-\xi\rho}{(\xi+\eta)^{\rho+1}} \tag{3.13}$$

$$\frac{\partial S_2}{\partial\eta} = \frac{-\xi\rho}{(\xi+\eta)^{\rho+1}} \tag{3.14}$$

$$\frac{\partial S_3}{\partial\xi} = \frac{-\xi\rho}{(\xi+\eta)^{\rho+1}} \tag{3.15}$$

$$\frac{\partial S_3}{\partial\eta} = \frac{\xi+\eta-\eta\rho}{(\xi+\eta)^{\rho+1}} \tag{3.16}$$

while the first derivatives of ξ and η over x and y are

$$\frac{\partial\xi}{\partial x} = \frac{1}{2A_e}b_2 \tag{3.17}$$

$$\frac{\partial\xi}{\partial x} = \frac{1}{2A_e}c_2 \tag{3.18}$$

$$\frac{\partial\eta}{\partial y} = \frac{1}{2A_e}b_3 \tag{3.19}$$

$$\frac{\partial\eta}{\partial y} = \frac{1}{2A_e}c_3. \tag{3.20}$$

The derivatives component of each shape function can be obtained by combining the derivative forms in (3.11) - (3.16) with those in (3.17)- (3.20) and substituting into the (3.9).

$$\frac{\partial S_1}{\partial x} = \frac{(\rho-1)(b_2+b_3)}{2A_e(\xi+\eta)^\rho} \tag{3.21}$$

$$\frac{\partial S_1}{\partial y} = \frac{(\rho-1)(c_2+c_3)}{2A_e(\xi+\eta)^\rho} \tag{3.22}$$

$$\frac{\partial S_2}{\partial x} = \frac{b_2(\xi+\eta-\xi\rho)-b_3\xi\rho}{2A_e(\xi+\eta)^{\rho+1}} \quad (3.23)$$

$$\frac{\partial S_2}{\partial y} = \frac{c_2(\xi+\eta-\xi\rho)-c_3\xi\rho}{2A_e(\xi+\eta)^{\rho+1}} \quad (3.24)$$

$$\frac{\partial S_3}{\partial x} = \frac{b_3(\xi+\eta-\eta\rho)-b_2\xi\rho}{2A_e(\xi+\eta)^{\rho+1}} \quad (3.25)$$

$$\frac{\partial S_3}{\partial y} = \frac{c_3(\xi+\eta-\eta\rho)-c_2\xi\rho}{2A_e(\xi+\eta)^{\rho+1}} \quad (3.26)$$

Substituting those derivations into the second integral in RHS of (3.4) and the numerical solution by using Gauss quadrature integral approximations is

$$\begin{aligned}\frac{w}{k^2}\iint_{A_e} \nabla S_i \cdot \nabla S_j \, dA_e &= \frac{w}{k^2}\int_0^1\int_0^{1-\xi} \nabla S_i(\xi,\eta)\cdot\nabla S_j(\xi,\eta)\, d\eta d\xi \\ &= \frac{w}{k^2}|J|\cdot\sum_{i=1}^{n} w_i \nabla S_i(\xi,\eta)\cdot\nabla S_j(\xi,\eta). \quad (3.27)\end{aligned}$$

To verify the accuracy of this integral approximation, it compares the calculation result of the analytical integral of standard element to the numerical integral of the singular element with $\rho = 0$. Using the manner that the singular element shape function behaves as a standard element when $\rho = 0$. The first integral comparison listed on Table 3.1 shows that the results are quite similar, while the results of the second integral listed on table 3.2 have a bit disagreement, but it is still acceptable for the analysis.

Table 3.1: Comparison of the first integral calculations

Integrand	Analytical	Numerical	% Error
S_1S_1	3.0396782E-06	3.0396782E-06	0
S_1S_2	1.5198391E-06	1.5198391E-06	0
S_1S_3	1.5198391E-06	1.5198391E-06	0
S_2S_1	1.5198391E-06	1.5198391E-06	0
S_2S_2	3.0396782E-06	3.0396782E-06	0
S_2S_3	1.5198391E-06	1.5198391E-06	0
S_3S_1	1.5198391E-06	1.5198391E-06	0
S_3S_2	1.5198391E-06	1.5198391E-06	0
S_3S_3	3.0396782E-06	3.0396782E-06	0

Table 3.2: Comparison of the second integral calculations

Integrand	Analytical	Numerical	% Error
$\nabla S_1 \cdot \nabla S_1$	2.2456357E-02	2.2456355E-02	8.9E-06
$\nabla S_1 \cdot \nabla S_2$	-2.0557465E-02	-2.0557463E-02	9.7E-06
$\nabla S_1 \cdot \nabla S_3$	-1.8988920E-03	-1.8988930E-03	5.3E-05
$\nabla S_2 \cdot \nabla S_1$	-2.0557465E-02	-2.0557463E-02	9.7E-06
$\nabla S_2 \cdot \nabla S_2$	4.6254300E-02	4.6254292E-02	1.7E-05
$\nabla S_2 \cdot \nabla S_3$	-2.5696833E-02	-2.5696832E-02	3.9E-06
$\nabla S_3 \cdot \nabla S_1$	-1.8988920E-03	-1.8988930E-03	5.3E-05
$\nabla S_4 \cdot \nabla S_2$	-2.5696833E-02	-2.5696832E-02	3.9E-06
$\nabla S_3 \cdot \nabla S_3$	2.7595725E-02	2.7595727E-02	7.2E-06

3.3.2 Singular element on the internal surface integrals

The singular element shape function is also utilized in the elements around the corner that have two nodes on the internal surface. Therefore, the surface integrals related with these elements must use a line shape function that has compatibility to the singular element shape function. The expression in (3.1) is modified to be one-dimensional form by assuming $S_3 = 0$ and replacing S_1 and S_2 with N_1 and N_2 in (2.34).

$$N_{s-1}(u)^l = 1 - N_2^{1-\rho} \tag{3.28}$$

$$N_{s-2}(u)^l = N_2^{1-\rho} \tag{3.29}$$

The shape function of two internal surface integrals in (2.37) and (2.38) is replaced by the singular shape function.

$$H_i^{e_{int}} = \frac{1}{j\omega\epsilon_0}\iint_{S_i} H_u^{inc} N_{s-i}(u) \cos\alpha \, ds \tag{3.30}$$

$$Y_{ij}^{(e_{int})} = \iint_{S_j}\iint_{S_i} N_{s-i}(u) \cos\alpha \; \hat{u} \cdot \overline{\overline{G}}_{int}(\overline{r}, \overline{r}') \cdot \hat{u}' \; N_{s-j}(u') \cos\alpha' \; ds'ds \tag{3.31}$$

Table 3.3: Comparison of H_i calculations

Slot Part	Node(i)	Real/Imag	Analytical	Numerical	% error
bottom	1	real	-2.8409957E-04	-2.8410213E-04	9.0E-4
		imag	-2.4511071E-03	-2.4511290E-03	8.9E-4
bottom	2	real	-1.4213145E-04	-1.4212899E-04	1.7E-3
		imag	-1.2262581E-03	-1.2262367E-03	1.7E-3
side	1	real	-1.2702153E-02	-1.2702722E-02	4.4E-3
		imag	1.6365291E-03	1.6366213E-03	5.6E-3
side	2	real	-1.2681411E-02	-1.2680837E-02	4.5E-3
		imag	1.7984287E-03	1.7983522E-03	4.2E-3
top	1	real	-5.8931054E-04	-5.8930030E-04	1.7E-3
		imag	-1.0847227E-03	-1.0847037E-03	1.7E-3
top	2	real	-1.1779438E-03	-1.1779543E-03	8.9E-4
		imag	-2.1681988E-03	-2.1682181E-03	8.9E-4

Table 3.4: Comparison of the Y_{ij} calculations

Node (i)	Node(j)	Real/Imag	Analytical	Numerical	% error
1	1	real	4.2778217E-07	4.2668734E-07	0.2
		imag	-1.7326905E-09	-1.7327213E-09	1.8E-3
1	2	real	2.4878821E-07	2.4846693E-07	0.1
		imag	-8.6684332E-10	-8.6683588E-10	8.6E-4
2	1	real	2.4878821E-07	2.4846693E-07	0.1
		imag	-8.6684332E-10	-8.6683588E-10	8.6E-4
2	2	real	1.7739590E-07	1.7596315E-07	0.8
		imag	-4.3367085E-10	-4.3365564E-10	3.5E-3

The ρ-squared function also makes the integrals become difficult to be solved analytically. Thus these integrals are solved by using the Gauss quadrature integral approximation for a line integral. The approximation is verified by comparing the analytical solution of integral with standard element to the numerical approximation of $\rho = 0$ singular element, as shown in Table 3.3 and 3.4 for H_i and Y_{ij}, respectively. The comparisons show that the numerical integration has a good accuracy.